



Constraints on global oceanic emissions of N₂O from observations and models

Erik T. Buitenhuis^{1,2}, Parvatha Suntharalingam¹, and Corinne Le Quééré^{1,2}

¹School of Environmental Sciences, University of East Anglia, Norwich, UK

²Tyndall Centre for Climate Change Research, University of East Anglia, Norwich, UK

Correspondence: Erik T. Buitenhuis (e031@uea.ac.uk)

Received: 16 May 2017 – Discussion started: 19 May 2017

Revised: 7 March 2018 – Accepted: 11 March 2018 – Published: 13 April 2018

Abstract. We estimate the global ocean N₂O flux to the atmosphere and its confidence interval using a statistical method based on model perturbation simulations and their fit to a database of $\Delta p\text{N}_2\text{O}$ ($n = 6136$). We evaluate two submodels of N₂O production. The first submodel splits N₂O production into oxic and hypoxic pathways following previous publications. The second submodel explicitly represents the redox transformations of N that lead to N₂O production (nitrification and hypoxic denitrification) and N₂O consumption (suboxic denitrification), and is presented here for the first time. We perturb both submodels by modifying the key parameters of the N₂O cycling pathways (nitrification rates; NH₄⁺ uptake; N₂O yields under oxic, hypoxic and suboxic conditions) and determine a set of optimal model parameters by minimisation of a cost function against four databases of N cycle observations. Our estimate of the global oceanic N₂O flux resulting from this cost function minimisation derived from observed and model $\Delta p\text{N}_2\text{O}$ concentrations is 2.4 ± 0.8 and $2.5 \pm 0.8 \text{ Tg N yr}^{-1}$ for the two N₂O submodels. These estimates suggest that the currently available observational data of surface $\Delta p\text{N}_2\text{O}$ constrain the global N₂O flux to a narrower range relative to the large range of results presented in the latest IPCC report.

tive understanding of the magnitude and processes controlling natural N₂O emissions from the Earth surface to the atmosphere is very poor. A range of methods have been used to constrain total oceanic N₂O emissions, including the combination of surface ocean N₂O partial pressure anomalies with gas-exchange parameterisations (Nevison et al., 1995), empirically derived functional relationships applied to global ocean datasets (Nevison et al., 2003; Freing et al., 2012), and ocean biogeochemistry models (Suntharalingam and Sarmiento, 2000; Suntharalingam et al., 2000; Jin and Gruber, 2003; Martinez-Rey et al., 2015). In spite of the multiple methods used, the reported oceanic emissions of N₂O are still poorly constrained, ranging from 1.9 to 9.4 Tg N yr⁻¹ according to the latest report of the Intergovernmental Panel on Climate Change (IPCC; Ciais et al., 2013). The uncertainty in the oceanic emissions of N₂O accounts for a large part of the total uncertainty in the natural N₂O emissions, which is approximately 11 Tg N yr⁻¹ (Ciais et al., 2013). Part of the uncertainty in the oceanic emissions is whether estuaries are included, which could emit as much as 2.3–3.6 Tg N yr⁻¹ (Bange et al., 1996).

The large uncertainty in the oceanic emissions of N₂O stems from the complexity of its production pathways. There are two main pathways of N₂O production in the ocean, nitrification and denitrification, which both stem from redox reactions of nitrogen, under oxic and hypoxic conditions, respectively (Fig. 1). N₂O is formed as a byproduct of marine nitrification of ammonium (NH₄⁺) to nitrate (NO₃⁻); N₂O is also an intermediate product of denitrification, during the reduction of NO₃⁻ to nitrogen gas (N₂) (Frame and Casciotti, 2010; Loescher et al., 2012; Merbt et al., 2012). Denitrification can also consume N₂O,

1 Introduction

Nitrous oxide (N₂O) is the third-most important contributor to anthropogenic radiative forcing, after carbon dioxide (CO₂) and methane (CH₄) (Myhre et al., 2013). It is also currently estimated as the dominant contributor to stratospheric ozone depletion (Portmann et al., 2012). Yet our quantita-

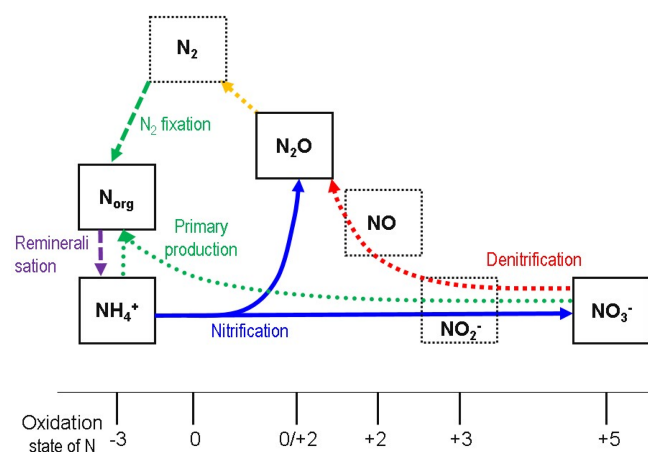


Figure 1. Primary biological pathways of the oceanic nitrogen N cycle represented in the model simulations, along with redox states of N. Nitrification occurs in the oxic ocean (blue arrow). Denitrification yields net N₂O production in hypoxic conditions (red arrow) and net N₂O consumption in suboxic conditions (yellow arrow). Only organic nitrogen (N_{org}), NH₄⁺, NO₃⁻ and N₂O are represented as model state variables.

using extracellular N₂O, and reduce it to N₂ (Bange, 2008). In the oxic part of the ocean (i.e. most of the ocean, 97 % > 34 μmol O₂ L⁻¹, using O₂ data taken from Bianchi et al., 2012) denitrification is suppressed, and the primary formation pathway is usually ascribed to nitrification (Cohen and Gordon, 1978), although denitrification may be significant in the anaerobic centres of large marine snow particles in oxic waters (Klawonn et al., 2015). Oceanic N₂O production in oxic regions is often derived from the linear relationships observed between apparent oxygen utilisation (AOU) and apparent N₂O production (ΔN₂O) (e.g. Yoshinari, 1976; Cohen and Gordon, 1978). However, the ΔN₂O / AOU ratio varies in different water masses and oceanic regions (Suntharalingam and Sarmiento, 2000). Previous studies have suggested that differences in the ΔN₂O / AOU ratio could be driven by changing N₂O yields under varying pressure and temperature (Butler et al., 1989) or varying O₂ concentration (Nevison et al., 2003). Additional mechanisms not yet quantified could include variations in the elemental stoichiometry of the organic matter that is being remineralised, and spatial separation of organic matter remineralisation and nitrification. Throughout the paper we will refer to N₂O stoichiometries relative to O₂, NH₄⁺ and NO₃⁻ as ratios, because they have been optimised against global databases of concentration measurements, rather than from microbiological yields. Using the latter would be more mechanistically satisfying, but the relevant yields are at present insufficiently constrained by observations.

Estimates of the contribution from suboxic regions of the ocean (about 3 %) to the global N₂O flux vary from net depletion via denitrification (Cohen and Gordon, 1978) to

33 % for the total N₂O production in the suboxic ocean (Suntharalingam et al., 2012) and to more than 50 % from denitrification alone (Yoshida et al., 1989). This ambiguity remains unresolved. Bottom-up microbial physiology data are relatively scarce (see Sect. 2.4–2.6), while top-down data need relatively complicated inverse methods to estimate the contribution from suboxic regions. These inverse methods are complicated both because of the variation in the ΔN₂O / AOU ratio, which is negative under suboxic conditions, maximal under hypoxic conditions and lower under oxic conditions (e.g. 0.31–0.033 mmol mol⁻¹, Law and Owens, 1990), and because of the influence of mixing gradients makes in situ ratios an unreliable gauge to the biological yields under in situ conditions (Nevison et al., 2003).

Here, we estimate the global ocean N₂O flux to the atmosphere and its confidence interval. First, we estimate N₂O flux from observations only (Sect. 2.1). This estimate has large uncertainty. We subsequently use a statistical approach introduced by Buitenhuis et al. (2013a) to estimate the global oceanic emissions of N₂O and its confidence interval by combining ocean N₂O model simulations with a global database of measurements of surface ΔpN₂O. This approach involves minimisation of a cost function that compares a series of model simulations with a global database of point measurements of surface ΔpN₂O. To achieve this, we use four observational databases of the N cycle (Sect. 2.2) to extend the global ocean biogeochemistry model PlankTOM10 (Le Quere et al., 2016b) with additional N cycle processes. We derive the biogeochemical parameters for nitrification rate and phytoplankton use of NH₄⁺ from the observational databases of nitrification rate and NH₄⁺ concentration (databases 1 and 2 and Sect. 2.4–2.5). Then, we describe two separate submodels of different levels of complexity that represent N₂O cycling pathways (Sect. 2.6–2.7). Finally, we apply the statistical approach (Sect. 2.8) to the two submodels to estimate the N₂O production in the low-O₂ regions from the depth resolved N₂O concentration database (database 3 and Sect. 3.1), and the global oceanic N₂O flux from the surface ΔpN₂O database (database 4 and Sect. 3.2), followed by a discussion of the results (Sect. 4).

2 Ocean N cycle

2.1 Calculation of global ocean N₂O production from N cycle observations

In this section we provide an initial estimate of global marine N₂O production based on observationally derived quantities characterising marine productivity and the global ocean N cycle. This follows a similar method to Cohen and Gordon (1979), who estimated ocean N₂O production using Redfield type ratios. N₂O is produced either during production of NO₃⁻ in NH₄⁺ oxidation or during NO₃⁻ reduction in denitrification (Fig. 1). We therefore base the

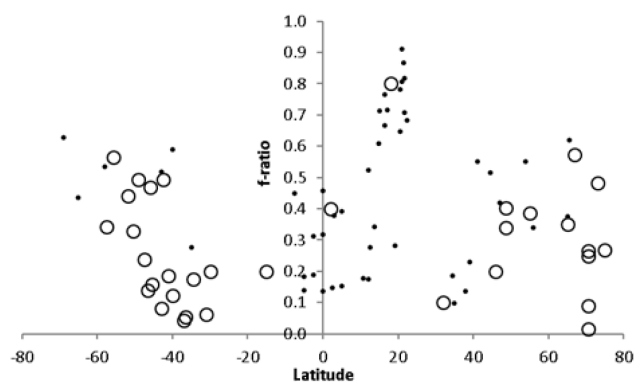


Figure 2. f ratio ($\rho_{\text{NO}_3^-} / (\rho_{\text{NO}_3^-} + \rho_{\text{NH}_4^+} + \rho_{\text{urea}})$) as a function of latitude, from ¹⁵N uptake experiments. Small dots were estimated without measuring NH_4^+ or urea concentrations (Prakash et al., 2008, 2015; Gandhi et al., 2010, 2012). Large dots did not give a significant linear relationship with absolute value of latitude and were therefore averaged at 0.29 ± 0.18 (Wafar et al., 2004; Varela et al., 2005, 2013; Joubert et al., 2011; Thomalla et al., 2011; Simpson et al., 2013).

N₂O production on total NO₃⁻ turnover, calculated from primary production times the f ratio. The f ratio is the fraction of primary production that is supported by nitrate. Primary production (PP) was estimated at $58 \pm 7 \text{ Pg C yr}^{-1}$ based on ¹⁴C primary production measurements ($n = 50\,050$), parameter perturbations of a previous version of the model used here, and Eq. (5) (Buitenhuis et al., 2013a). We compiled a database of uptake rates of NO₃⁻, NH₄⁺ and urea, which gives an average f ratio of 0.29 ± 0.18 (Fig. 2, large symbols, $n = 34$). The globally averaged $\Delta\text{N}_2\text{O} / \text{AOU}$ ratio was calculated from the MEMENTO database (Bange et al., 2009) as $81.5 \pm 1.4 \mu\text{mol} / \text{mol}$ (Fig. 3). Finally, since primary production is expressed in carbon terms, and N₂O production was correlated with oxygen (O₂) utilisation, we need to include the $-\text{O}_2 : \text{C}$ ratio (the $-$ sign indicates the O₂ is consumed as CO₂ is produced), which was taken from Anderson and Sarmiento (1994) as $170 \pm 10 / 117 \pm 14$, and the molar weights of C (12) and N in N₂O (28). Here and in the rest of the paper, errors were propagated in the usual way:

error =

$$\sqrt{\left(\frac{\text{error of } A}{A}\right)^2 + \left(\frac{\text{error of } B}{B}\right)^2 + \dots} \times A \times B \times \dots \quad (1)$$

Thus N₂O production was calculated as $\text{PP} \times f\text{ratio} \times -\text{O}_2 : \text{C} \times \Delta\text{N}_2\text{O} / \text{AOU}$. Our best estimate of N₂O production using this method is $58 \pm 7 \times 1000 \times 0.29 \pm 0.18 \times 170 \pm 10 / 117 \pm 14 \times 81.5 \times 10^{-6} \pm 1.4 \times 10^{-6} \times 28 / 12 = 4.6 \pm 3.1 \text{ Tg N yr}^{-1}$. This estimate lies in the middle of other reported estimates (Fig. 4), but the 68% confidence interval is very large. We therefore investigate the N₂O fluxes using a model optimised with observations in the rest of the paper.

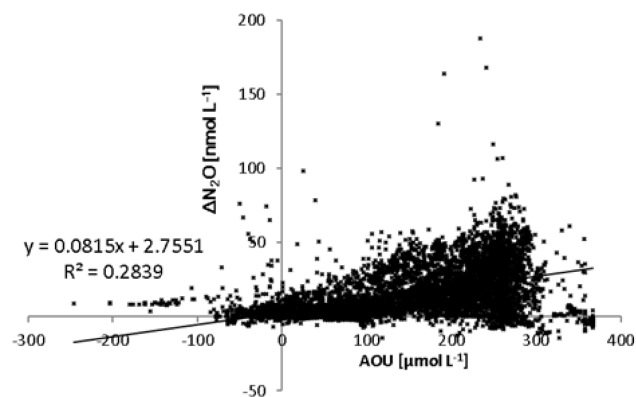


Figure 3. Apparent N₂O production ($\Delta\text{N}_2\text{O} \text{ nmol L}^{-1}$) as a function of apparent oxygen utilisation (AOU $\mu\text{mol L}^{-1}$).

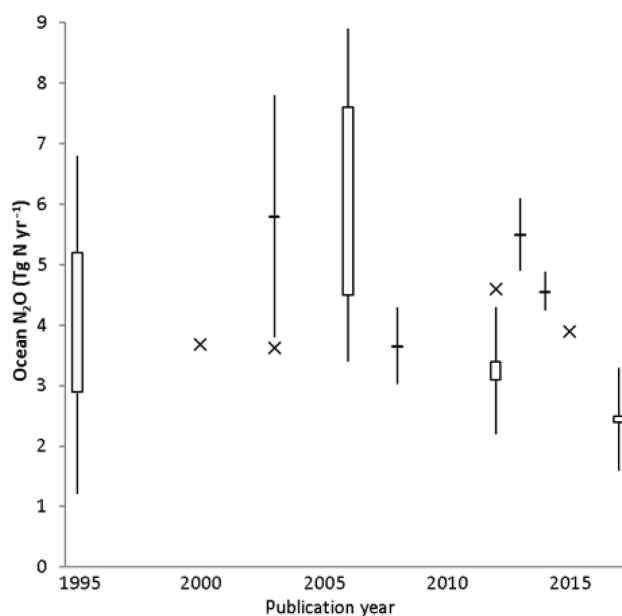


Figure 4. Published estimates of global ocean N₂O production or air–sea exchange. Estimates based on global observational datasets shown as boxes when ranges are given and whiskers if error estimates are given (ocean observations: Nevison et al., 1995; Nevison et al., 2003; Freing et al., 2012 (plotted in 2011); Bianchi et al., 2012; this study – atmospheric inversions: Hirsch et al., 2006; Huang et al., 2008; Thompson et al., 2014 (plotted in 2013); Saikawa et al., 2014), model estimates shown as crosses (Suntharalingam and Sarmiento, 2000; Jin and Gruber, 2003; Suntharalingam et al., 2012; Martinez-Rey et al., 2015).

2.2 Observational databases for model development

We used four databases to tune or optimise different aspects of the N cycle in the PlankTOM10 ocean biogeochemistry model. The number of data points reported for each database are after gridding to $1^\circ \times 1^\circ \times 12 \text{ months} \times 33 \text{ depths}$ (World Ocean Atlas 2009). The databases used are (1) NH₄⁺ spe-

cific nitrification rate (d^{-1} , raw data $n = 425$, gridded data $n = 296$) as described in Yool et al. (2007); (2) surface NH_4^+ concentration distribution ($\mu\text{mol L}^{-1}$, raw data $n = 33\,079$, gridded data $n = 23\,433$) that combines the dataset used in Paulot et al. (2015) with data held by the British Oceanographic Data Centre (Martin Johnson, personal communication, 2015, <http://www.bodc.ac.uk>, last access: January 2014); (3) depth-resolved N_2O concentration from the MEMENTO project (nmol L^{-1} , <https://memento.geomar.de/>; Bange et al., 2009; downloaded 4 June 2014, raw data $n = 14\,342$, gridded data $n = 8047$); and (4) surface partial pressure of N_2O ($p\text{N}_2\text{O}$) also from MEMENTO (ppb, downloaded 16 September 2015, raw data $n = 227\,463$, gridded data $n = 6136$). Since there is at present no formal quality control beyond that performed by individual contributors to the MEMENTO database and a check by the database administrators that the values make physical sense (Kock and Bange, 2015), we have taken the database at face value. $p\text{N}_2\text{O}$ was converted to $\Delta p\text{N}_2\text{O}$ using atmospheric $p\text{N}_2\text{O}$:

$$p\text{N}_2\text{O}_{\text{atm}} = 0.00009471353 \times Y^3 - 0.052147139 \times Y^2 + 95.68066 \times Y - 58228.41 \quad (2)$$

(Alina Freing, personal communication, 2014, correction to Freing et al., 2009), in which Y is the decimal year. The average absolute difference relative to the global average $p\text{N}_2\text{O}_{\text{atm}}$ data from the NOAA/ESRL Global Monitoring Division (ftp://ftp.cmdl.noaa.gov/hats/n2o/combined/HATS_global_N2O.txt, last access: 8 June 2017) is 0.5 ppb between 1977 and 2014 and 0.3 ppb between 2000 and 2014.

2.3 Cost function formulation

To parameterise the model N cycle, we use a cost function to minimise the difference between model and observations, following the methods of Buitenhuis et al. (2013a):

$$\text{cost function} = 10^{\sum |\log_{10}(\text{model}/\text{observation})|/n} \quad (3)$$

This formulation gives equal weight to the relative correspondence between model and observations at small and large observational values. A value of 2 means that, on average, the model deviates from the observations by a factor 2 in either direction. To calculate the cost function (and also to calculate MSE in Eq. 6), the model was regridded to the same grid as the observations, and residuals were calculated at months and places where there are observations. The cost function results for the optimised simulations are summarised in Table 1.

2.4 Nitrification

Our initial biogeochemical model configuration is PlankTOM10 (Le Quere et al., 2016b), which represents growth and loss terms from 10 plankton functional types (PFTs), including N_2 fixers, picoheterotrophs (*Bacteria* plus *Archaea*)

and denitrification rate, but not denitrifier biomass. A full model description and parameter values are provided in the Supplement. Here, we extend the model representation of redox reactions in the N cycle, to create the global biogeochemical model PlankTOM10.2. We describe the new N cycle components below.

In order to represent nitrification rate, the state variable for dissolved inorganic nitrogen was split into NO_3^- and NH_4^+ . Respiration by all PFTs produces NH_4^+ . The parameterisation for nitrification used in our model is based on the analysis of a database of NH_4^+ -specific nitrification rates (Yool et al., 2007). Yool et al. (2007) found that observed nitrification rates are highly variable, with no obvious relationship with either latitude or depth. In their model they therefore used a constant rate of 0.2 d^{-1} throughout the ocean. Implementing this rate in our model resulted in a cost function relative to the nitrification rate observations of 4.22 (Table 1). We tested if including temperature, O_2 or light dependence improves the ability of the model to reproduce observed nitrification rates. Regarding the response of ammonia-oxidising *Archaea* (AOA), the main nitrifiers in the ocean (Francis et al., 2005; Wuchter et al., 2006; Loescher et al., 2012), to temperature, we are only aware of the measurements of Qin et al. (2014). These show a ~ 4 -fold variation in maximum growth rate between three strains, which poorly constrains the temperature dependence of AOA. We therefore first used a generic Q_{10} of 2 and optimised the rate at 0°C using the nitrification rate observations. This led to only a slightly improved representation of the observations (cost function = 4.18). Although the response of AOA and ammonia-oxidising *Bacteria* (AOB) to O_2 has only been measured at 21 – 25°C (Frame and Casciotti, 2010; Loescher et al., 2012), which limits the range of O_2 concentrations, there was a significant logarithmic relationship between N_2O yield and O_2 (Fig. 5). A logarithmic function fitted the data better than linear, exponential or power functions. Since nitrification consumes O_2 , in the model it decreases as remineralisation switches from O_2 to NO_3^- (Eqs. 61, 67 and 70 in the Supplement). Implementing this response to O_2 led to only a further small improvement of the model nitrification rate relative to the observations (cost = 4.16). This implies that nitrification never becomes O_2 limited, reflecting a lack of data to parameterise an expected decrease. As will be described more fully in Sect. 3.1, we used observed O_2 concentrations in the simulations (Bianchi et al., 2012) rather than interactively modelled O_2 to minimise the impact of model biases in simulated O_2 fields (Suntharalingam et al., 2012). The response of AOA to light is estimated to be 50% inhibited at $5 \mu\text{mol photons m}^{-2} \text{ s}^{-1}$. However, this estimate is not well constrained (Merbt et al., 2012). Implementing this light response did not improve the model, either in combination with the O_2 and temperature responses or with the temperature response only, and was subsequently omitted. The lack of improvement in nitrification rates by adding light inhibi-

tion might reflect the lower sensitivity of AOA to light found by Qin et al. (2014).

2.5 Phytoplankton $K_{1/2}$ for NH_4^+ uptake

We used the calculation of the preferential uptake of NH_4^+ over NO_3^- by phytoplankton PFTs of Vallina and Le Quere (2008) (Eq. 9 in the Supplement). The $K_{1/2}$ of phytoplankton for NH_4^+ has mostly been measured based on uptake rates (syntheses by Goldman and Glibert, 1983; Killberg-Thoreson et al., 2014). Aksnes and Egge (1991) have shown a theoretical expectation of a linear increase of $K_{1/2}$ with cell radius. The observations are so variable that they neither confirm nor contradict such an increase. The model uses a fixed C : N : O₂ ratio for all organic matter of 122 : 16 : -172, and Michaelis–Menten kinetics for growth based on inorganic N uptake by phytoplankton (Buitenhuis et al., 2013a; Eqs. 8 and 9 in the Supplement). We therefore need a $K_{1/2}$ for growth rather than for uptake to be consistent with the fixed C : N ratio (Morel, 1987). The available uptake rate data do not include the supporting data to allow conversion to the $K_{1/2}$ for growth. We are only aware of measurements of the $K_{1/2}$ for growth by Stawiarski (2014). Based on the latter values of $0.09 \pm 0.15 \mu\text{mol L}^{-1}$ for picoeukaryotes, the $K_{1/2}$ of phytoplankton for NH_4^+ was set to 0.1 to $5 \mu\text{mol L}^{-1}$, increasing linearly with nominal size (Buitenhuis et al., 2013b). Due to the highly dynamic nature of NH_4^+ turnover, the model produces a much smoother distribution of NH_4^+ concentrations than the observations, but the large-scale pattern of surface NH_4^+ concentration shows an increase with latitude, consistent with the observations (Fig. 6), which translates into a cost function of 3.0.

2.6 N₂O production

N₂O production is implemented as two distinct submodels. The diagnostic submodel is based on statistical relationships of $\Delta\text{N}_2\text{O} / \text{AOU}$ ratios taken from observations and has previously been published (Suntharalingam et al., 2000, 2012). In oxic waters it uses one ratio to estimate the open ocean source of N₂O production. In hypoxic waters it uses a higher ratio to represent the increased yield of N₂O from both nitrification and denitrification in oxygen minimum zones. The hypoxic N₂O yield is maximal at $1 \mu\text{mol O}_2 \text{ L}^{-1}$, and decreases with an e -folding concentration of $10 \mu\text{mol O}_2 \text{ L}^{-1}$ (Suntharalingam et al., 2000, 2012; Eqs. 35, 67 and 69 in the Supplement). Previous studies using regional databases have found different oxic ratios (Suntharalingam and Sarmiento, 2000, and references therein). Therefore, both the oxic and hypoxic ratios have been reoptimised to the global databases (Sect. 3.1–3.2).

The prognostic submodel presented here is based on process understanding and explicitly represents the primary N₂O formation and consumption pathways associated with the marine nitrogen cycle (Fig. 1). It includes the production of

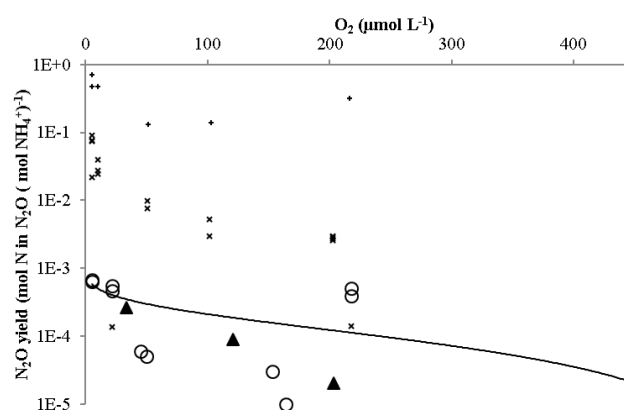


Figure 5. N₂O yield of nitrification (N atom : atom) as a function of O₂ concentration; filled triangles: AOA (Loescher et al., 2012); open circles: AOB at low to medium cell numbers (Frame and Casciotti, 2010; Loescher et al., 2012); crosses: marine AOB at high cell numbers (Goreau et al., 1980; Frame and Casciotti, 2010); pluses: soil AOB at high cell numbers (Lipschultz et al., 1981). Black line: logarithmic fit to AOA and low to medium cell number AOB (yield = $0.791 - 0.126 \cdot \ln(\text{O}_2) \text{ mmol N in N}_2\text{O (mol NH}_4^+)^{-1}$).

N₂O during oxic nitrification (blue arrows in Fig. 1) and during hypoxic denitrification (red arrow in Fig. 1), as well as a consumption term during denitrification at even lower (sub-oxic) O₂ concentrations (yellow arrow in Fig. 1). The ratios of the three processes are globally invariant (Eqs. 61, 63, 70 and 71 in the Supplement). The functional form of the O₂ dependence of N₂O consumption (Eq. 71 in the Supplement) was the same as that of denitrification (Eq. 67 in the Supplement), and with an O₂ response function that is $1.5 \mu\text{mol L}^{-1}$ lower than that of denitrification, which is similar to that used by Babbín et al. (2015). We independently optimised the ratios of N₂O production and consumption from denitrification (Sect. 3.1), which controls the net N₂O production as a function of O₂ concentration. There is not enough information at present to optimise the O₂ concentration parameters of denitrification and N₂O consumption as well. The low O₂ ratios of both submodels (Supplement Sect. 8.7) were optimised using the database of observed N₂O concentration (Sect. 3.1) and the oxic ratios of both submodels were optimised using the database of observed $\Delta p\text{N}_2\text{O}$ (Sect. 3.2). The N₂O concentrations from both the diagnostic and the prognostic submodels are transported in the same way by physical transport, and the formulation of their gas exchange is also identical.

Table 1. Cost function (Eq. 3) for the optimisation simulations of Sect. 2.2–2.4, relative to the respective observational databases. The nitrification rate in bold was used in this study.

Database	Model change	Cost function
Nitrification rate	0.2 d^{-1}	4.22
	$0.1 \text{ d}^{-1} \times 2^{(T/10)}$	4.18
	$0.79 \text{ d}^{-1} \times 2^{(T/10)} \times (1 - 0.159 \times \ln(\text{O}_2))$	4.16
	$0.58 \text{ d}^{-1} \times 2^{(T/10)} \times e^{(-0.14 \times I)}$	7.15
	$4.7 \text{ d}^{-1} \times 2^{(T/10)} \times (1 - 0.159 \times \ln(\text{O}_2)) \times e^{(-0.14 \times I)}$	6.87
Surface NH ₄ ⁺ concentration	K _{1/2} estimated from observations	3.0

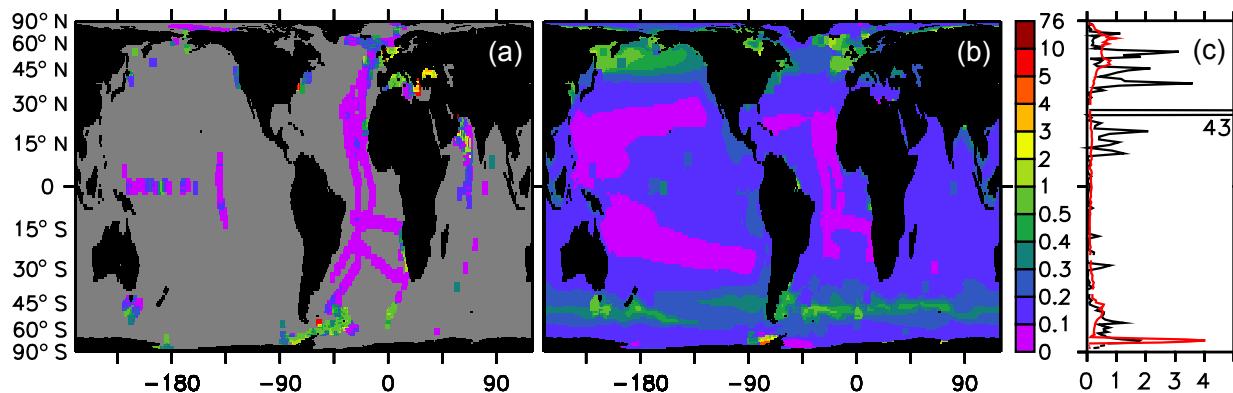


Figure 6. Surface NH₄⁺ concentration ($\mu\text{mol L}^{-1}$). (a) Observations (symbol size is $5^\circ \times 5^\circ$). (b) Model results are for the same months where there are observations, and annual averages everywhere else. (c) Zonal average. Black: observations; red: model results. Model results are for the same months and longitudes as the observations. Latitude y axis to the left of panel (a).

2.7 N₂O flux and simulation setup

N₂O is transported like other tracers. N₂O flux (= air–sea gas exchange) is calculated as

$$\begin{aligned} \text{N}_2\text{O flux} = & (p\text{N}_2\text{O}_{\text{atm}} \times K0 \times (1 - p_{\text{watervapour}}) - p\text{N}_2\text{O}) \\ & \times \text{piston_velocity} \times \sqrt{660/\text{Schmidt_number}_{\text{N}_2\text{O}}} \\ & \times (1 - \text{ice_cover}), \end{aligned} \quad (4)$$

in which $K0$ is the solubility (Weiss and Price, 1980), $p_{\text{watervapour}}$ is the water vapour pressure (Sarmiento et al., 1992), $\text{piston_velocity} = 0.27 \times (\text{windspeed})^2$ (Sweeney et al., 2007), which is optimised for use with the NCEP reanalysis data used here, the Schmidt number for N₂O was taken from Wanninkhof (1992), and the ice cover is calculated by the sea ice model LIM2.

In most of the simulations, atmospheric $p\text{N}_2\text{O}$ was calculated from Eq. (2). For the optimised low O₂ production we also ran a series of simulations with the NOAA $p\text{N}_2\text{O}_{\text{atm}}$ observational data that included seasonal and latitudinal variations (see Sect. 2.2 for the ftp address where we downloaded the data, and Sect. 3.2 for the results). Between 2000 and 2014, we used the monthly observations for the 12 available latitudes. Monthly anomalies relative to the global average were calculated at each available latitude from the 2000–

2016 observations. These were added to Eq. (2) from 1965 and 1976, and to the global average observations between 1977 and 1999. In the model simulation, the data were linearly interpolated between the 12 latitudes and monthly observations.

The PlankTOM10.2 biogeochemical model coupled with the two N₂O submodels is incorporated into the ocean general circulation model NEMO v3.1 (Madec, 2008). The model resolution is 2° in longitude, on average 1.1° in latitude and has 30 vertical layers, from 10 m in the top 100 m to 500 m at 5000 m. The model simulations were initialised in 1965 from observations (Le Quere et al., 2016b), with NH₄⁺ initialised as 0, and N₂O initialised from a horizontal interpolation of the MEMENTO observations (see Sect. 2.2). Simulations were run to 2014, forced with daily atmospheric conditions from the NCEP reanalysis (Kalnay et al., 1996; for details see Buitenhuis et al., 2013a). Results are reported averaged over the last 5 years.

2.8 Estimation of global N₂O flux from point measurements of $\Delta p\text{N}_2\text{O}$

In previous versions of the PlankTOM model (Buitenhuis et al., 2006, 2010, 2013a) we have used Eq. (3) to evaluate the model because it minimises relative error, which we have

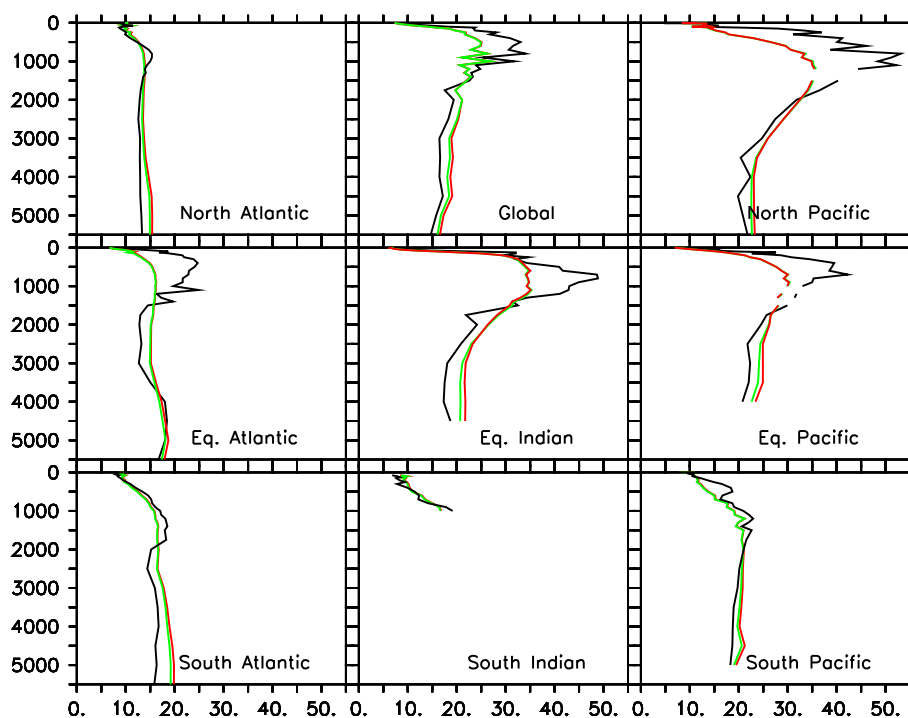


Figure 7. Depth profiles of N₂O concentration (nmol L⁻¹) for different basins. Black lines: observations; green lines: optimised diagnostic model; red lines: optimised prognostic model.

found to be more appropriate when the observations span several orders of magnitude. Unfortunately, statistical confidence intervals have only been defined for χ^2 statistics such as Eqs. (5) and (6), which minimise absolute error, so that we end up with two cost functions (Eqs. 3 and 5), depending on the application. To estimate the global air–sea flux of N₂O that best fits the $\Delta p\text{N}_2\text{O}$ data, and its ± 1 –sigma (68 %) confidence interval, we use the formula described in Buitenhuis et al. (2013a):

$$\text{MSE}/\text{MSE}_{\min} = 0.468 \times n/(n-2) \times \sqrt{(2(2n-2)/(n(n-4))) + n/(n-2)}, \quad (5)$$

in which MSE is mean square error:

$$\text{MSE} = \frac{\sum (\text{model}(\text{longitude, latitude, month}) - \text{observation}(\text{longitude, latitude, month}))^2}{n}. \quad (6)$$

MSE_{\min} is the MSE of the model simulation that is closest to the observations, and n is the number of gridded observations.

In addition to the uncertainty that arises from the model–observations mismatch, uncertainty is contributed by the uncertainties in the N₂O solubility and the piston velocity, the two quantities that connect the measured $\Delta p\text{N}_2\text{O}$ to the estimated air–sea flux. The uncertainty in the solubility has been estimated as 3 % (Cohen and Gordon, 1978). The uncertainty

in the piston velocity has been estimated at 32 % (Sweeney et al., 2007). Uncertainties in the solubility and piston velocity are proportional to uncertainty in the optimised N₂O air–sea exchange because the optimised N₂O production needs to change proportionally with solubility and piston velocity to achieve the same $\Delta p\text{N}_2\text{O}$.

3 Results

3.1 N₂O production at low O₂

The global N₂O production rate in oxygen minimum zones (OMZs) was optimised using the depth-resolved N₂O data of the MEMENTO database. As noted in previous model studies of ocean O₂, global models do not well represent the extent and intensity of OMZ regions (Bopp et al., 2013; Cocco et al., 2013). The modelled OMZs in PlankTOM10 occur at greater depths than observed, resulting in unrealistic vertical distributions of N₂O (results not shown). Therefore, following Suntharalingam et al. (2012), the model was run using fixed observed O₂ concentrations (Bianchi et al., 2012), which corrected, in part, the vertical distribution of N₂O production from the two submodels, though it still occurred at too great depths (Fig. 7). In the equatorial regions and in the Pacific Ocean the N₂O concentrations are underestimated between ~ 200 and ~ 1500 m depth, and overestimated below that. This shortcoming is not significantly improved in the

prognostic model (Fig. 7), even though the prognostic model is more detailed, separately representing the processes of N₂O production and consumption at low O₂ concentrations. The depth of maximum N₂O in the model is generally deeper than observed, suggesting that organic matter remineralisation may be too low at shallow depths. This is confirmed by the depth profile of NO₃⁻, which is underestimated relative to the WOA2009 observations between 100 and 1500 m, and overestimated at greater depths (Fig. 8). In both submodels, the N₂O concentrations in the deep sea are also too high, but since only 5 % of N₂O production occurs below 1600 m this does not have a big impact on the global N₂O fluxes. The addition of N₂O consumption in the prognostic N₂O model does result in improvement of the N₂O depth profiles in the Indian Ocean.

In order to find the optimal N₂O production that minimises the MSE (Eq. 5), we ran a range of simulations in which the low-O₂ N₂O production was varied in the diagnostic model (Fig. 9a), and a range of simulations in which both the hypoxic N₂O production and the suboxic N₂O consumption were varied in the prognostic model (Fig. 9b). The optimum solution for the prognostic model was found at a gross production of 0.33 Tg N yr⁻¹. The optimised (net) N₂O production in low-O₂ regions and its confidence interval were 0.16 ± 0.13 Tg N yr⁻¹ for the diagnostic model, and 0.12 ± 0.07 Tg N yr⁻¹ for the prognostic model. In the optimised diagnostic model the hypoxic N₂O ratio (i.e. net production) is 1.7 mmol N₂O (mol O₂)⁻¹. In the optimised prognostic model the maximum N₂O production ratio (i.e. gross production from hypoxic denitrification) is 15.4 mmol N₂O (mol NO₃⁻)⁻¹, decreasing to 0 above 34 μmol O₂ L⁻¹. The maximum N₂O consumption ratio (from suboxic denitrification) is 15 mmol N₂O (mol NO₃⁻)⁻¹, decreasing to 0 above 28 μmol O₂ L⁻¹. This leads to net production that is always positive and has a maximal ratio of 183 μmol N₂O (mol NO₃⁻)⁻¹ at 10 μmol O₂ L⁻¹.

3.2 N₂O flux

We used the surface Δ*p*N₂O distribution to constrain the total global N₂O flux, and the uncertainty arising from the model–data mismatch (the uncertainties arising from solubility and piston velocity are added at the end). We ran a range of simulations in which both the (net) low O₂ and the oxic N₂O production rates were optimised in both submodels (Fig. 10). Δ*p*N₂O provided a better constraint than the N₂O concentration distribution, since more N₂O production mostly leads to more N₂O outgassing to the atmosphere rather than a significant increase in shallow N₂O concentrations (data not shown). This is because outgassing is proportional to Δ*p*N₂O, but N₂O concentration is proportional to *p*N₂O, and Δ*p*N₂O / *p*N₂O is small in most of the surface ocean. The zonal average surface Δ*p*N₂O distribution was well simulated by both submodels (Fig. 11d), and the model ensemble covered a wide range of global N₂O

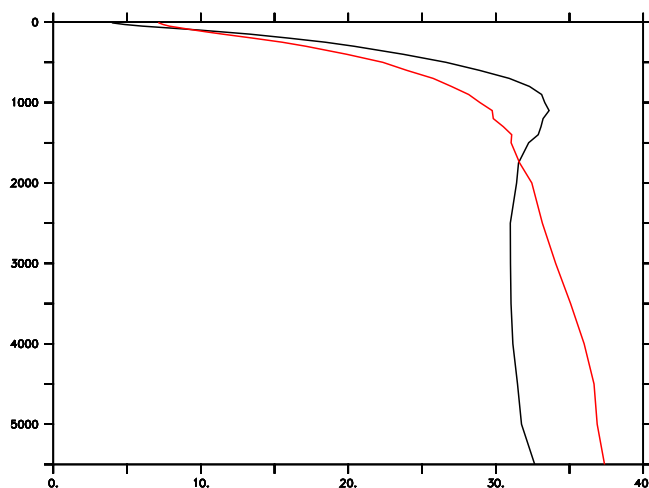


Figure 8. Depth (m) profile of average NO₃⁻ concentration (μmol L⁻¹). Black line: WOA2009 synthesis of observations, not interpolated. Red line: model results sampled at the places where there are observations.

fluxes (Fig. 10). The total N₂O flux that best reproduced the Δ*p*N₂O distribution was 2.4 ± 0.3 Tg N yr⁻¹ for the diagnostic submodel and 2.5 ± 0.3 Tg N yr⁻¹ for the prognostic submodel (Fig. 10). In the diagnostic model, the optimised oxic ΔN₂O / AOU ratio was 10.6 μmol N₂O (mol O₂)⁻¹. In the prognostic model, the optimised oxic nitrification ratio was 123 μmol N₂O (mol NH₄⁺)⁻¹. The results were the same in both diagnostic and prognostic submodels for the 2000–2004 and 2005–2009 averages, showing that the model was sufficiently spun up.

High N₂O fluxes have been reported for the coastal ocean (Bange et al., 1996), and near-shore upwelling regions (e.g. Arevalo-Martinez et al., 2015). To test whether these regions contribute more to the global N₂O flux than their surface area would suggest, we did the optimisation separately for the coastal ocean (≤ 200 m bottom depth) for the near-shore non-coastal ocean (≤ 2° from land, > 200 m bottom depth) for the eastern tropical Pacific (180–70° W, 5° S–5° N, > 2° from land) and the rest of the open ocean (Table 2). The results show that the coastal ocean contributes only 2 % of the global N₂O flux, less than would be expected from its surface area, although there are also fewer observations on the coast (2 % of the total), so that the relative error is slightly higher. The near-shore non-coastal ocean contributes 14 % of the global N₂O flux both submodels, hardly more than its areal percentage (13 %), and it is also fairly well sampled (12 % of the observations). The eastern equatorial Pacific Ocean contributes 27 % in the diagnostic submodel and 25 % in the prognostic model, more than its areal percentage (22 %), and it is undersampled (17 %). The open ocean contributes 57–59 %, slightly less than its areal percentage (61 %). This is as expected, because we have separated out the main N₂O hotspots, but the differences are quite small.

When we used observed atmospheric $p\text{N}_2\text{O}$ that varied with latitude and month (see Sect. 2.2) the results were essentially the same, with an N₂O flux of $2.4 \pm 0.3 \text{ Tg N yr}^{-1}$ for the diagnostic submodel and $2.6 \pm 0.3 \text{ Tg N yr}^{-1}$ for the prognostic submodel (data not shown).

Finally, we add the uncertainties in the solubility and the piston velocity to the total N₂O flux through error propagation. This gives a total uncertainty of $2.4 \pm 0.8 \text{ Tg N yr}^{-1}$ for the diagnostic submodel and $2.5 \pm 0.8 \text{ Tg N yr}^{-1}$ for the prognostic submodel.

4 Discussion

Cohen and Gordon (1979) estimated global N₂O production directly from N cycle observations as $4\text{--}10 \text{ Tg N yr}^{-1}$. However, they did not have information on the f ratio, so their estimate was based on total N assimilation in primary production. We use an updated estimate of primary production and its error (Buitenhuis et al., 2013a), and compile a database of the f ratio (Fig. 2). We also use a much larger database of the $\Delta\text{N}_2\text{O} / \text{AOU}$ ratio (Fig. 3). We recalculate the N-cycle-based N₂O production based on these extended databases. We find that we can estimate all the relevant steps in the N cycle with observational data, including their uncertainty (Sect. 2.1). At present this uncertainty is still fairly large, at $4.6 \pm 3.1 \text{ Tg N yr}^{-1}$. The uncertainty in this estimate is similar to that in Cohen and Gordon (1979), but our uncertainty is based on the uncertainty in all components of the calculation, while their uncertainty was based only on the uncertainty in the $\Delta\text{N}_2\text{O} / \text{AOU}$ ratio. The upper 60 % of our estimate overlaps with the lower 62 % of the Cohen and Gordon (1979) estimate. The biggest contributor to our uncertainty is the f ratio, especially in the tropics, which constitute 44 % of the ocean surface area, and additional measurements and/or data synthesis could help constrain the N₂O budget. The f -ratio data are only based on uptake of NO_3^- , NH_4^+ and urea, whereas phytoplankton can also take up NO_2^- and organic N (other than urea). One of the major sources of uncertainty in using the $\Delta\text{N}_2\text{O} / \text{AOU}$ ratio is that it is conceptually based on the N₂O production during nitrification, which uses O₂ as the electron acceptor. N₂O production during denitrification is spatially separated from the associated O₂ use that is needed to nitrify the NH_4^+ to NO_3^- , the electron acceptor in denitrification. This NO_3^- is produced by nitrification, so in terms of mass balance our calculation is still valid, but this N₂O production would show up as a vertical increase in N₂O without associated increase in AOU at low O₂ concentrations (high AOU) in Fig. 4. This estimate of global marine N₂O production derived from analysing the N cycle ($4.6 \pm 3.1 \text{ Tg N yr}^{-1}$) is statistically indistinguishable from the N₂O flux derived from $\Delta p\text{N}_2\text{O}$ observations ($2.4\text{--}2.5 \pm 0.8 \text{ Tg N yr}^{-1}$) but has a much larger error. However, further observational constraints could not only reduce the error but also extend our understanding of

the whole N cycle, including the option of evaluating the model representation of these N cycle processes against observations, and not just the part that N₂O plays in them. Such further constraints are also likely to provide the most productive way to reduce unexplained variability that is found in the observations but not in the present models. For example, we have shown that both the N₂O and NO₃ are underestimated at $\sim 300\text{--}1500 \text{ m}$ depth and overestimated below $\sim 2000 \text{ m}$ (Figs. 6 and 7). Thus, improved representation of mesopelagic remineralisation might lead in improved representation of the N₂O depth distribution. However, this falls outside the scope of this study.

Models of the global marine C cycle have been in use for decades, and a lot of the available information has been synthesised, cross-correlated and interpreted in detail (Le Quere et al., 2016a; Buitenhuis et al., 2013b). While actual measurements of N utilisation and transformation have also been made in abundance (Figs. 2, 3, 4, 5a, 6, 7 and 9a), the synthesis and global modelling of these data are less advanced. In addition, N occurs in many different oxidation states in the marine environment (e.g. organic matter and NH_4^+ as -3 , N₂ as 0 , N₂O as 0 and $+2$, NO_2^- as $+3$, and NO_3^- as $+5$). Therefore, redox reactions complicate the representation of the N cycle a good deal. This lack of data synthesis and of identification of the most important controls in a complex system is reflected in a relatively low ability of the model to model observed nitrification rates and to a lesser extent NH_4^+ concentrations (Table 1).

This lack of knowledge also means that partitioning the global marine N₂O production over the nitrification and denitrification pathways is poorly constrained. Both the diagnostic and the prognostic models assign a small percentage of the total N₂O production to the denitrification pathway, 6 and 4 % respectively. However, because of the large bias between the observed and modelled N₂O concentration depth profiles (Fig. 7) these may be underestimates (Suntharalingam et al., 2012; Arevalo-Martinez et al., 2015). Possibly because of the model bias (Figs. 7 and 8), the addition of N₂O consumption in the prognostic submodel does not lead to a significantly better distribution of N₂O across depth or between different basins (Fig. 8). As a result, the $\Delta p\text{N}_2\text{O}$ distributions are also quite similar (Figs. 11 and 12) and the optimised N₂O flux and confidence intervals of the two submodels are also quite similar (Fig. 10). However, it should also be noted, first, that the optimisation using surface $\Delta p\text{N}_2\text{O}$ agrees with the optimisation using N₂O concentration that the contribution of the low-O₂ N₂O production needs to be low (Fig. 10). Second, the error contribution from the model vs. observed $\Delta p\text{N}_2\text{O}$ comparison is low, with confidence intervals of 0.3 Tg N yr^{-1} for both submodels. Third, $\Delta p\text{N}_2\text{O}$ is equally well modelled above the low-O₂ regions as in the rest of the ocean (Figs. 11 and 12), and the contributions of the coastal and near-shore non-coastal ocean are nearly proportional to their surface areas (Table 2). These three features are supporting evidence for our results that suggest that

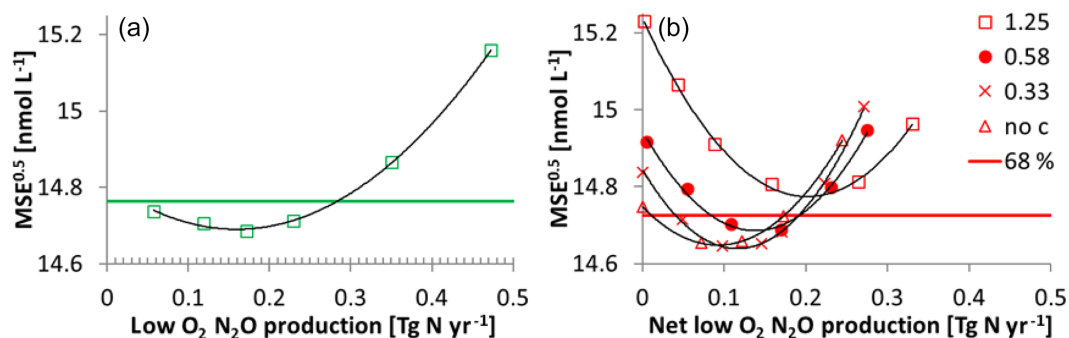


Figure 9. $\text{MSE}^{0.5}$ for the two N₂O submodels compared to the N₂O concentration database as a function N₂O production in the low-O₂ regions. MSE_{\min} was obtained as the minimum of a second-order polynomial fit (black lines). The 1σ confidence interval, where MSE equals the value calculated from Eq. (5), is indicated by the horizontal lines. (a) Diagnostic submodel; each point represents a simulation with a different low O₂ ratio. (b) Prognostic model; “no c” is with no N₂O consumption, i.e. net production = gross production. All other lines have a constant gross production (see legend for a description of the symbols, Tg N yr⁻¹), and net production varies with different N₂O consumption rates. Range of parameter values is given in Supplement Sect. 8.7.

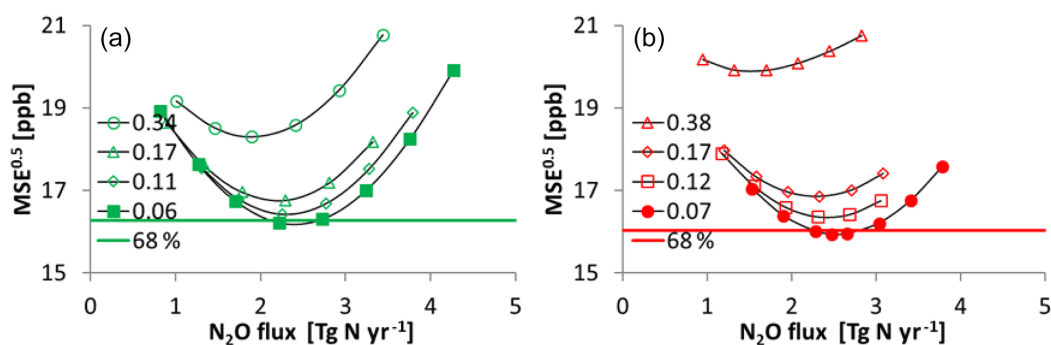


Figure 10. $\text{MSE}^{0.5}$ for the two N₂O submodels compared to the $\Delta p\text{N}_2\text{O}$ database as a function of global N₂O flux at different (net) N₂O production rates in the low-O₂ regions. MSE_{\min} and confidence intervals as in Fig. 9. (a) Diagnostic submodel. The four lines represent the four best low O₂ production rates from Fig. 9a; each point represents a simulation, different symbols indicate different low O₂ ratios, and points with the same symbols have different oxic N₂O production ratios. (b) Prognostic submodel. The four lines represent the optimised net production rates at the four best gross production rates from Fig. 9b; points with the same symbols have different N₂O ratios for nitrification.

the low-O₂ regions make a small contribution to the global ocean N₂O production. They should be balanced against the model bias of the vertical distribution of N₂O concentrations, which suggests a larger contribution from the low-O₂ regions. Freing et al. (2012) also estimated a small fraction of 7 % of the global total contributed by denitrification/low-O₂ N₂O production. Two complementary approaches could provide better constraints: a better representation of the vertical distribution of export and remineralisation would allow the optimisation against N₂O concentration observations to achieve better results. But, conversely, with better constraints on the physiology of nitrifiers and denitrifiers the N₂O concentration database could provide constraints on the representation of remineralisation. Although there are relatively few N₂O concentration observations, nitrification and denitrification respond to specific environmental queues (in particular O₂ concentration), so that they could contribute a rel-

atively large observational constraint over the full range of environmental conditions.

Despite these shortcomings, the global marine N₂O flux is well constrained to $2.4\text{--}2.5 \pm 0.8 \text{ Tg N yr}^{-1}$ by both submodels (Fig. 10). This constraint reflects the fact that the integrated effect of the different physical and biogeochemical processes determines the surface $\Delta p\text{N}_2\text{O}$ distribution (Fig. 11), so that the integrated total can be well constrained even if the individual processes are not. The N₂O flux is at the lower end of previous estimates, and with a similar confidence interval to other recent estimates (Fig. 4). The confidence interval is dominated by uncertainty in the piston velocity (32 %) rather than model–observation mismatches (12 %). Because of differences in methodology it is not possible to provide reasons for why our estimate is lower than the more recent estimates. We can, however, compare our estimate to that of Nevison et al. (1995), because it is also based on a database of $\Delta p\text{N}_2\text{O}$. Compared

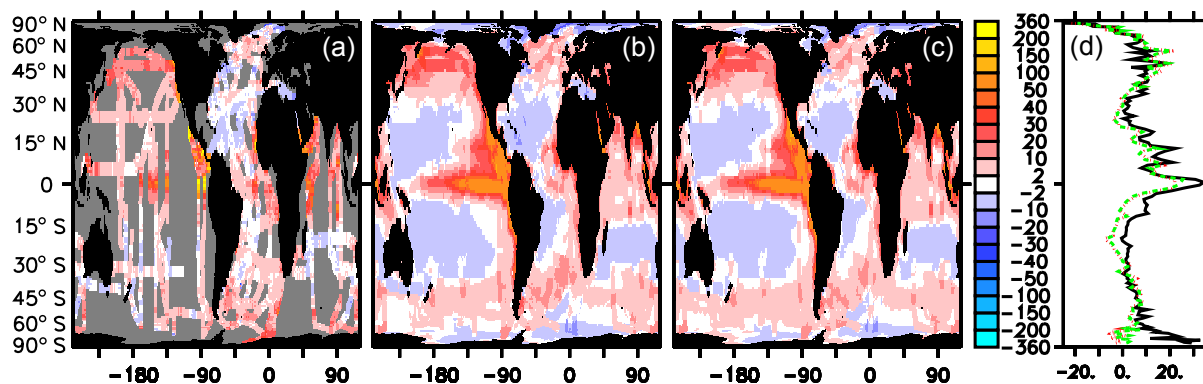


Figure 11. Surface $\Delta p\text{N}_2\text{O}$ (ppb). (a) Observations (symbol size is $5^\circ \times 5^\circ$). (b) Optimised diagnostic model. (c) Optimised prognostic model. Model results are for the same months where there are observations, and annual averages everywhere else. (d) Zonal average. Black line: observations; green dashed: diagnostic model; red dotted: prognostic model. Model results are for the same months and longitudes as the observations. Latitude y axis to the left of panel (a).

Table 2. Contributions of coastal (bottom depth ≤ 200 m), near-shore non-coastal ($\leq 2^\circ$ from land, bottom depth > 200 m), eastern equatorial Pacific ($180\text{--}70^\circ$ W 5° S– 5° N, $> 2^\circ$ from land) and rest of the open ocean ($> 2^\circ$ from land, bottom depth > 200 m, excluding eastern equatorial Pacific) to N₂O flux, area and number of observations.

Region	Submodel	N ₂ O flux	% N ₂ O flux	% area	% n_{obs}
Coastal ocean	Diagnostic	0.05 ± 0.01	2	5	2
	Prognostic	0.041 ± 0.007	2		
Deep offshore	Diagnostic	0.33 ± 0.04	14	13	12
	Prognostic	0.37 ± 0.04	14		
East. eq. Pac.	Diagnostic	0.64 ± 0.05	27	22	17
	Prognostic	0.67 ± 0.05	25		
Open ocean	Diagnostic	1.37 ± 0.19	57	61	69
	Prognostic	1.54 ± 0.21	59		

to their high-end estimate using the piston velocity of Wanninkhof of $5.2 \pm 3.6 \text{ Tg N yr}^{-1}$, our estimate is lower because we use the more recent 13 % lower estimate of piston velocity of Sweeney et al. (2007), and because our $\Delta p\text{N}_2\text{O}$ of 7.6 ± 18.1 ppb is 25–28 % lower compared to 10.55 natm in Nevison et al. (1995) (the range is calculated based on the water vapour correction for conversion between ppb and natm, which increases from 0.6 to 4.1 % at temperatures from 0 to 30 °C, which brings the values slightly closer together).

We also tested how much influence sampling biases of very high supersaturation values might have on the estimated air–sea exchange. If the 40 $\Delta p\text{N}_2\text{O}$ measurements in the gridded database that are higher than 100 ppb (Fig. 12) are doubled, the optimised N₂O air–sea exchange becomes $2.8 \pm 0.5 \text{ Tg N yr}^{-1}$ for the diagnostic model and $3.1 \pm 0.5 \text{ Tg N yr}^{-1}$ for the prognostic model. If the 24 $\Delta p\text{N}_2\text{O}$ measurements in the gridded database that are higher than 152 ppm are excluded, to decrease the frequency of the highly oversaturated observations down to what both submodels simulate (Fig. 12), the optimised

N₂O flux becomes 2.0 ± 0.2 for the diagnostic model and $2.3 \pm 0.2 \text{ Tg N yr}^{-1}$ for the prognostic model. These results still fall within the confidence intervals of the results using the complete database.

Possible biases in ocean physical transport could in theory affect N₂O production in low-O₂ regions. The indirect impact of ocean physics on low N₂O production through its impact on the distribution of O₂, which Zamora and Oschlies (2014) have shown to be substantial, is not quantified here because we used observed O₂ (Bianchi et al., 2012) instead of modelled O₂. Our model results suggest that the model representation of ocean physics is adequate for the purpose of estimating N₂O flux from biogeochemical model perturbations. On the one hand, if the model had too much ventilation in the OMZs, shallow N₂O concentrations would be underestimated, as they are in the model (Fig. 7), but this would also lead to $\Delta p\text{N}_2\text{O}$ overestimation in the surface areas above the OMZs, which is not the case. The high $\Delta p\text{N}_2\text{O}$ values are generally lower but spread over a larger area than in the observations (Fig. 11), with a good frequency distri-

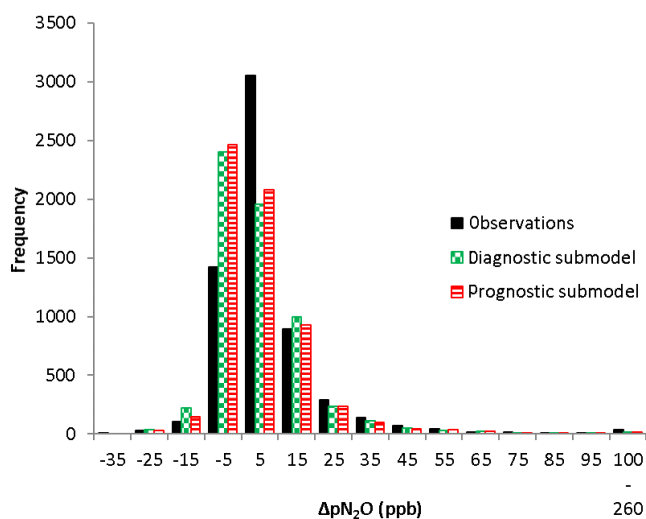


Figure 12. Frequency distribution of $\Delta p\text{N}_2\text{O}$ in the observations (solid black), and the optimised simulations of the diagnostic submodel (green squares) and the prognostic submodel (red lines).

bution of high $\Delta p\text{N}_2\text{O}$ (Fig. 12). On the other hand, if the model had too little ventilation in the OMZs, the optimisation would reduce N₂O production in the OMZs in compensation, but the optimisation to $\Delta p\text{N}_2\text{O}$ would then estimate a higher OMZ N₂O production than the optimisation to the N₂O depth profiles to compensate for the low transport, and this is also not the case. Therefore we conclude that potential biases in ocean physical transport do not appear to have a large direct impact on low N₂O production.

Global oceanic N₂O emissions estimated using atmospheric inversion methods based on atmospheric N₂O concentrations tend to be higher than our results (Fig. 4). However, N₂O emissions from inversions in the Southern Ocean are lower than the priors (Hirsch et al., 2006; Huang et al., 2008; Thompson et al., 2014; Saikawa et al., 2014). These low Southern Ocean emissions (0.02–0.72 Tg N yr⁻¹) are consistent with our results (0.68–0.79 Tg N yr⁻¹). South of 30° S, 88 % of the Earth surface is ocean, resulting in a clearer attribution in the inversions of the atmospheric N₂O anomalies to ocean fluxes. We suggest that the higher emissions estimates from inversions for the global ocean could be due to a combination of overestimated priors of ocean fluxes in combination with insufficient observational constraints at latitudes north of 30° S to allow correct partitioning between land and ocean fluxes. Results presented here are for the open and coastal ocean. The largest coastal seas are resolved in our model, although specific coastal processes, such as the interactions with sediments and tides, are not. Our results do not include emissions from estuaries. Fluxes from these could be as large as 2.3–3.6 Tg N yr⁻¹ according to one estimate (Bange et al., 1996), and could be another contributing factor to the difference between our results and those of atmospheric inversions.

To improve the estimate of the ocean N₂O flux, first, the uncertainty in the piston velocity would need to be reduced. Once that is achieved, further improvements might be possible by a more accurate model representations of the remineralisation length scale and of the physiology of N₂O producing picoheterotrophs (nitrifying and denitrifying *Archaea* and *Bacteria*).

Code and data availability. The four databases presented in this paper are available as NetCDF files from <https://www.uea.ac.uk/green-ocean/data>. The code of PlankTOM10.2 is available at greenocean-data.uea.ac.uk/model/PlankTOM10.2.tar.

The Supplement related to this article is available online at <https://doi.org/10.5194/bg-15-2161-2018-supplement>.

Competing interests. The authors declare that they have no conflict of interest.

Acknowledgements. This research was supported by the European Commission's Horizon 2020 programme through the CRESCENDO and EMBRACE projects (projects 641816 and 282672). We thank Martin Johnson for the database of NH₄⁺, and Andrew Yool for the database of nitrification rates. The MEMENTO database is administered by the Kiel Data Management Team at GEOMAR Helmholtz Centre for Ocean Research and supported by the German BMBF project SOPRAN (Surface Ocean Processes in the Anthropocene, <http://sopran.pangaea.de>, last access: 10 April 2018). We thank Alina Freing for providing the corrected numbers for the polynomial fit to the atmospheric $p\text{N}_2\text{O}$ data, and NOAA for providing atmospheric $p\text{N}_2\text{O}$ data.

Edited by: Syed Wajih Ahmad Naqvi

Reviewed by: three anonymous referees

References

- Aksnes, D. and Egge, J.: A theoretical-model for nutrient-uptake in phytoplankton, *Mar. Ecol. Prog. Ser.*, 70, 65–72, <https://doi.org/10.3354/meps070065>, 1991.
- Anderson, L. and Sarmiento, J.: Redfield ratios of remineralization determined by nutrient data-analysis, *Global Biogeochem. Cy.*, 8, 65–80, <https://doi.org/10.1029/93GB03318>, 1994.
- Arevalo-Martinez, D. L., Kock, A., Loescher, C. R., Schmitz, R. A., and Bange, H. W.: Massive nitrous oxide emissions from the tropical South Pacific Ocean, *Nat. Geosci.*, 8, 530–533, <https://doi.org/10.1038/NGEO2469>, 2015.
- Babbín, A. R., Bianchi, D., Jayakumar, A., and Ward, B. B.: Rapid nitrous oxide cycling in the suboxic ocean, *Science*, 348, 1127–1129, <https://doi.org/10.1126/science.aaa8380>, 2015.

- Bange, H.: Gaseous nitrogen compounds (NO, N₂O, N₂, NH₃) in the ocean, in: Nitrogen in the marine environment, edited by: Capone, D. G., Bronk, D. A., Mulholland, M. R., and Carpenter, E. J., Elsevier, Amsterdam, 51–94, 2008.
- Bange, H., Rapsomanikis, S., and Andreae, M.: Nitrous oxide in coastal waters, *Global Biogeochem. Cy.*, 10, 197–207, <https://doi.org/10.1029/95GB03834>, 1996.
- Bange, H. W., Bell, T. G., Cornejo, M., Freing, A., Uher, G., Upstill-Goddard, R. C., and Zhang, G.: MEMENTO: a proposal to develop a database of marine nitrous oxide and methane measurements, *Environ. Chem.*, 6, 195–197, <https://doi.org/10.1071/EN09033>, 2009.
- Bianchi, D., Dunne, J. P., Sarmiento, J. L., and Galbraith, E. D.: Data-based estimates of suboxia, denitrification, and N₂O production in the ocean and their sensitivities to dissolved O₂, *Global Biogeochem. Cy.*, 26, GB2009, <https://doi.org/10.1029/2011GB004209>, 2012.
- Bopp, L., Resplandy, L., Orr, J. C., Doney, S. C., Dunne, J. P., Gehlen, M., Halloran, P., Heinze, C., Ilyina, T., Séférian, R., Tjiputra, J., and Vichi, M.: Multiple stressors of ocean ecosystems in the 21st century: projections with CMIP5 models, *Biogeosciences*, 10, 6225–6245, <https://doi.org/10.5194/bg-10-6225-2013>, 2013.
- Buitenhuis, E.: PlankTOM10.2 code, available at: greenocean-data.uea.ac.uk/model/PlankTOM10.2.tar, last access: 10 April 2018.
- Buitenhuis, E., Le Quere, C., Aumont, O., Beaugrand, G., Bunker, A., Hirst, A., Ikeda, T., O'Brien, T., Piontkovski, S., and Straile, D.: Biogeochemical fluxes through mesozooplankton, *Global Biogeochem. Cy.*, 20, GB2003, <https://doi.org/10.1029/2005GB002511>, 2006.
- Buitenhuis, E. T., Rivkin, R. B., Sailley, S., and Le Quere, C.: Biogeochemical fluxes through microzooplankton, *Global Biogeochem. Cy.*, 24, GB4015, <https://doi.org/10.1029/2009GB003601>, 2010.
- Buitenhuis, E. T., Hashioka, T., and Le Quere, C.: Combined constraints on global ocean primary production using observations and models, *Global Biogeochem. Cy.*, 27, 847–858, <https://doi.org/10.1002/gbc.20074>, 2013a.
- Buitenhuis, E. T., Vogt, M., Moriarty, R., Bednaršek, N., Doney, S. C., Leblanc, K., Le Quéré, C., Luo, Y.-W., O'Brien, C., O'Brien, T., Peloquin, J., Schiebel, R., and Swan, C.: MAREDAT: towards a world atlas of MARine Ecosystem DATA, *Earth Syst. Sci. Data*, 5, 227–239, <https://doi.org/10.5194/essd-5-227-2013>, 2013b.
- Butler, J., Elkins, J., Thompson, T., and Egan, K.: Trophospheric and dissolved N₂O of the West Pacific and East-Indian Oceans during the El-Niño Southern Oscillation event of 1987, *J. Geophys. Res.-Atmos.*, 94, 14865–14877, <https://doi.org/10.1029/JD094iD12p14865>, 1989.
- Ciais, P., Sabine, C., Bala, G., Bopp, L., Brovkin, V., Canadell, J., Chhabra, A., DeFries, R., Heimann, M., Jones, C., Le Quere, C., Myneni, B., Piao, S., and Thornton, P.: Carbon and other biogeochemical cycles, in: Climate change 2013: The physical science basis, edited by: Stocker, T. F., Qin, D., Plattner, M., Tignor, M., Allen, S. K., Boschung, J., Nauels, Y., Xia, Y., Bex, V., and Midgley, P. M., 465–570, Cambridge University Press, New York, <https://doi.org/10.1017/CBO9781107415324.015>, 2013.
- Cocco, V., Joos, F., Steinacher, M., Frölicher, T. L., Bopp, L., Dunne, J., Gehlen, M., Heinze, C., Orr, J., Oschlies, A., Schneider, B., Segsneider, J., and Tjiputra, J.: Oxygen and indicators of stress for marine life in multi-model global warming projections, *Biogeosciences*, 10, 1849–1868, <https://doi.org/10.5194/bg-10-1849-2013>, 2013.
- Cohen, Y. and Gordon, L.: Nitrous-oxide in oxygen minimum of eastern tropical North Pacific - evidence for its consumption during denitrification and possible mechanisms for its production, *Deep-Sea Res.*, 25, 509–524, [https://doi.org/10.1016/0146-6291\(78\)90640-9](https://doi.org/10.1016/0146-6291(78)90640-9), 1978.
- Cohen, Y. and Gordon, L.: Nitrous-oxide production in the ocean, *J. Geophys. Res.-Oc. Atm.*, 84, 347–353, <https://doi.org/10.1029/JC084iC01p00347>, 1979.
- Frame, C. H. and Casciotti, K. L.: Biogeochemical controls and isotopic signatures of nitrous oxide production by a marine ammonia-oxidizing bacterium, *Biogeosciences*, 7, 2695–2709, <https://doi.org/10.5194/bg-7-2695-2010>, 2010.
- Francis, C., Roberts, K., Beman, J., Santoro, A., and Oakley, B.: Ubiquity and diversity of ammonia-oxidizing archaea in water columns and sediments of the ocean, *P. Natl. Acad. Sci. USA*, 102, 14683–14688, <https://doi.org/10.1073/pnas.0506625102>, 2005.
- Freing, A., Wallace, D. W. R., Tanhua, T., Walter, S., and Bange, H. W.: North Atlantic production of nitrous oxide in the context of changing atmospheric levels, *Global Biogeochem. Cy.*, 23, GB4015, <https://doi.org/10.1029/2009GB003472>, 2009.
- Freing, A., Wallace, D. W. R., and Bange, H. W.: Global oceanic production of nitrous oxide, *Philos. T. Roy. Soc. B.*, 367, 1245–1255, <https://doi.org/10.1098/rstb.2011.0360>, 2012.
- Gandhi, N., Prakash, S., Ramesh, R., and Kumar, S.: Nitrogen uptake rates and new production in the northern Indian Ocean, *Indian J. Mar. Sci.*, 39, 362–368, 2010.
- Gandhi, N., Ramesh, R., Laskar, A. H., Sheshshayee, M. S., Shetye, S., Anilkumar, N., Patil, S. M., and Mohan, R.: Zonal variability in primary production and nitrogen uptake rates in the southwestern Indian Ocean and the Southern Ocean, *Deep-Sea Res.*, 67, 32–43, <https://doi.org/10.1016/j.dsr.2012.05.003>, 2012.
- Goldman, J. and Glibert, P. M.: Kinetics of inorganic nitrogen uptake by phytoplankton, in: Nitrogen in the marine environment, edited by: Carpenter, E. J. and Capone, D. G., Academic Press, New York, 1983.
- Goreau, T., Kaplan, W., Wofsy, S., McElroy, M., Valois, F., and Watson, S.: Production of NO₂- and N₂O by nitrifying bacteria at reduced concentrations of oxygen, *Appl. Environ. Microb.*, 40, 526–532, 1980.
- Green Ocean research group: Green Ocean Data, available at: <https://www.uea.ac.uk/green-ocean/data>, last access: 10 April 2018.
- Hirsch, A., Michalak, A., Bruhwiler, L., Peters, W., Dlugokencky, E., and Tans, P.: Inverse modeling estimates of the global nitrous oxide surface flux from 1998–2001, *Global Biogeochem. Cy.*, 20, GB1008, <https://doi.org/10.1029/2004GB002443>, 2006.
- Huang, J., Golombek, A., Prinn, R., Weiss, R., Fraser, P., Simmonds, P., Dlugokencky, E. J., Hall, B., Elkins, J., Steele, P., Langenfelds, R., Krummel, P., Dutton, G., and Porter, L.: Estimation of regional emissions of nitrous oxide from 1997 to 2005 using multinetwerk measurements, a chemical transport model, and an inverse method, *J. Geophys. Res.-Atmos.*, 113, D17313, <https://doi.org/10.1029/2007JD009381>, 2008.
- Jin, X. and Gruber, N.: Offsetting the radiative benefit of ocean iron fertilization by enhancing N₂O emissions, *Geophys. Res. Lett.*, 30, 2249, <https://doi.org/10.1029/2003GL018458>, 2003.

- Joubert, W. R., Thomalla, S. J., Waldron, H. N., Lucas, M. I., Boye, M., Le Moigne, F. A. C., Planchon, F., and Speich, S.: Nitrogen uptake by phytoplankton in the Atlantic sector of the Southern Ocean during late austral summer, *Biogeosciences*, 8, 2947–2959, <https://doi.org/10.5194/bg-8-2947-2011>, 2011.
- Kalnay, E., Kanamitsu, M., Kistler, R., Collins, W., Deaven, D., Gandin, L., Iredell, M., Saha, S., White, G., Woollen, J., Zhu, Y., Chelliah, M., Ebisuzaki, W., Higgins, W., Janowiak, J., Mo, K., Ropelewski, C., Wang, J., Leetmaa, A., Reynolds, R., Jenne, R., and Joseph, D.: The NCEP/NCAR 40-year reanalysis project, *B. Am. Meteorol. Soc.*, 77, 437–471, [https://doi.org/10.1175/1520-0477\(1996\)077<0437:TNYRP>2.0.CO;2](https://doi.org/10.1175/1520-0477(1996)077<0437:TNYRP>2.0.CO;2), 1996.
- Killberg-Thoreson, L., Mulholland, M. R., Heil, C. A., Sanderson, M. P., O'Neil, J. M., and Bronk, D. A.: Nitrogen uptake kinetics in field populations and cultured strains of *Karenia brevis*, *Harmful Algae*, 38, 73–85, <https://doi.org/10.1016/j.hal.2014.04.008>, 2014.
- Klawonn, I., Bonaglia, S., Bruchert, V., and Ploug, H.: Aerobic and anaerobic nitrogen transformation processes in N₂-fixing cyanobacterial aggregates, *Isme J.*, 9, 1456–1466, <https://doi.org/10.1038/ismej.2014.232>, 2015.
- Kock, A. and Bange, H.: Counting the ocean's greenhouse gas emissions, *EOS*, 96, 10–13, <https://doi.org/10.1029/2015EO023665>, 2015.
- Law, C. and Owens, N.: Significant flux of atmospheric nitrous oxide from the Northwest Indian-Ocean, *Nature*, 346, 826–828, <https://doi.org/10.1038/346826a0>, 1990.
- Le Quéré, C., Andrew, R. M., Canadell, J. G., Sitch, S., Korsbakken, J. I., Peters, G. P., Manning, A. C., Boden, T. A., Tans, P. P., Houghton, R. A., Keeling, R. F., Alin, S., Andrews, O. D., Anthoni, P., Barbero, L., Bopp, L., Chevallier, F., Chini, L. P., Ciais, P., Currie, K., Delire, C., Doney, S. C., Friedlingstein, P., Gkritzalis, T., Harris, I., Hauck, J., Haverd, V., Hoppema, M., Klein Goldewijk, K., Jain, A. K., Kato, E., Körtzinger, A., Landschützer, P., Lefèvre, N., Lenton, A., Lienert, S., Lombardozi, D., Melton, J. R., Metzl, N., Millero, F., Monteiro, P. M. S., Munro, D. R., Nabel, J. E. M. S., Nakaoka, S.-I., O'Brien, K., Olsen, A., Omar, A. M., Ono, T., Pierrot, D., Poulter, B., Rödenbeck, C., Salisburry, J., Schuster, U., Schwinger, J., Séférian, R., Skjelvan, I., Stocker, B. D., Sutton, A. J., Takahashi, T., Tian, H., Tilbrook, B., van der Laan-Luijkx, I. T., van der Werf, G. R., Viovy, N., Walker, A. P., Wiltshire, A. J., and Zaehle, S.: Global Carbon Budget 2016, *Earth Syst. Sci. Data*, 8, 605–649, <https://doi.org/10.5194/essd-8-605-2016>, 2016a.
- Le Quéré, C., Buitenhuis, E. T., Moriarty, R., Alvain, S., Aumont, O., Bopp, L., Chollet, S., Enright, C., Franklin, D. J., Geider, R. J., Harrison, S. P., Hirst, A. G., Larsen, S., Legendre, L., Platt, T., Prentice, I. C., Rivkin, R. B., Sailley, S., Sathyendranath, S., Stephens, N., Vogt, M., and Vallina, S. M.: Role of zooplankton dynamics for Southern Ocean phytoplankton biomass and global biogeochemical cycles, *Biogeosciences*, 13, 4111–4133, <https://doi.org/10.5194/bg-13-4111-2016>, 2016b.
- Lipschultz, F., Zafriou, O., Wofsy, S., McElroy, M., Valois, F., and Watson, S.: Production of NO and N₂O by soil nitrifying bacteria, *Nature*, 294, 641–643, <https://doi.org/10.1038/294641a0>, 1981.
- Löscher, C. R., Kock, A., Könneke, M., LaRoche, J., Bange, H. W., and Schmitz, R. A.: Production of oceanic nitrous oxide by ammonia-oxidizing archaea, *Biogeosciences*, 9, 2419–2429, <https://doi.org/10.5194/bg-9-2419-2012>, 2012.
- Madec, G.: NEMO ocean engine, no. 27, Institute Pierre-Simon Laplace, 386 pp., France, 2008.
- Martinez-Rey, J., Bopp, L., Gehlen, M., Tagliabue, A., and Gruber, N.: Projections of oceanic N₂O emissions in the 21st century using the IPSL Earth system model, *Biogeosciences*, 12, 4133–4148, <https://doi.org/10.5194/bg-12-4133-2015>, 2015.
- Merbt, S. N., Stahl, D. A., Casamayor, E. O., Marti, E., Nicol, G. W., and Prosser, J. I.: Differential photoinhibition of bacterial and archaeal ammonia oxidation, *Fems Microbiol. Lett.*, 327, 41–46, <https://doi.org/10.1111/j.1574-6968.2011.02457.x>, 2012.
- Morel, F.: Kinetics of nutrient-uptake and growth in phytoplankton, *J. Phycol.*, 23, 137–150, 1987.
- Myhre, G., Shindell, D., Breon, F., Collins, W., Fuglestedt, J., Huang, J., Koch, D., Lamarque, J., Lee, D., Mendoza, T., Nakajima, A., Robock, A., Stephens, G., Takemura, T., and Zhang, H.: Anthropogenic and natural radiative forcing, in: *Climate change 2013: The physical science basis*, edited by: Stocker, T. F., Qin, D., Plattner, M., Tignor, M., Allen, S. K., Boschung, J., Nauels, Y., Xia, Y., Bex, V., and Midgley, P. M., 659–740, Cambridge University Press, New York, <https://doi.org/10.1017/CBO9781107415324.018>, 2013.
- Nevison, C., Weiss, R., and Erickson, D.: Global oceanic emissions of nitrous-oxide, *J. Geophys. Res.-Oceans*, 100, 15809–15820, <https://doi.org/10.1029/95JC00684>, 1995.
- Nevison, C., Butler, J., and Elkins, J.: Global distribution of N₂O and the Delta N₂O-AOU yield in the subsurface ocean, *Global Biogeochem. Cy.*, 17, 1119, <https://doi.org/10.1029/2003GB002068>, 2003.
- Paulot, F., Jacob, D. J., Johnson, M. T., Bell, T. G., Baker, A. R., Keene, W. C., Lima, I. D., Doney, S. C., and Stock, C. A.: Global oceanic emission of ammonia: Constraints from seawater and atmospheric observations, *Global Biogeochem. Cy.*, 29, 1165–1178, <https://doi.org/10.1002/2015GB005106>, 2015.
- Portmann, R. W., Daniel, J. S., and Ravishankara, A. R.: Stratospheric ozone depletion due to nitrous oxide: influences of other gases, *Philos. T. Roy. Soc. B.*, 367, 1256–1264, <https://doi.org/10.1098/rstb.2011.0377>, 2012.
- Prakash, S., Ramesh, R., Sheshshayee, M. S., Dwivedi, R. M., and Raman, M.: Quantification of new production during a winter *Noctiluca scintillans* bloom in the Arabian Sea, *Geophys. Res. Lett.*, 35, L08604, <https://doi.org/10.1029/2008GL033819>, 2008.
- Prakash, S., Ramesh, R., Sheshshayee, M. S., Mohan, R., and Sudhakar, M.: Nitrogen uptake rates and f-ratios in the Equatorial and Southern Indian Ocean, *Curr. Sci. India*, 108, 239–245, 2015.
- Qin, W., Amin, S. A., Martens-Habbena, W., Walker, C. B., Urakawa, H., Devol, A. H., Ingalls, A. E., Moffett, J. W., Armbrust, E. V., and Stahl, D. A.: Marine ammonia-oxidizing archaeal isolates display obligate mixotrophy and wide ecotypic variation, *P. Natl. Acad. Sci. USA*, 111, 12504–12509, <https://doi.org/10.1073/pnas.1324115111>, 2014.
- Saikawa, E., Prinn, R. G., Dlugokencky, E., Ishijima, K., Dutton, G. S., Hall, B. D., Langenfelds, R., Tohjima, Y., Machida, T., Manizza, M., Rigby, M., O'Doherty, S., Patra, P. K., Harth, C. M., Weiss, R. F., Krummel, P. B., van der Schoot, M., Fraser, P. J., Steele, L. P., Aoki, S., Nakazawa, T., and Elkins, J. W.: Global and regional emissions estimates for N₂O, At-

- mos. Chem. Phys., 14, 4617–4641, <https://doi.org/10.5194/acp-14-4617-2014>, 2014.
- Sarmiento, J., Orr, J., and Siegenthaler, U.: A perturbation simulation of CO₂ uptake in an ocean general-circulation model, *J. Geophys. Res.-Oceans*, 97, 3621–3645, <https://doi.org/10.1029/91JC02849>, 1992.
- Simpson, K. G., Tremblay, J.-E., Brugel, S., and Price, N. M.: Nutrient dynamics in the western Canadian Arctic, II. Estimates of new and regenerated production over the Mackenzie Shelf and Cape Bathurst Polynya, *Mar. Ecol.-Prog. Ser.*, 484, 47–62, <https://doi.org/10.3354/meps10298>, 2013.
- Stawiarski, B.: The physiological response of picophytoplankton to light, temperature and nutrients, including climate change model simulations, PhD. thesis, University of East Anglia, 157 pp., 2014.
- Suntharalingam, P. and Sarmiento, J.: Factors governing the oceanic nitrous oxide distribution: Simulations with an ocean general circulation model, *Global Biogeochem. Cy.*, 14, 429–454, <https://doi.org/10.1029/1999GB900032>, 2000.
- Suntharalingam, P., Sarmiento, J., and Toggeweiler, J.: Global significance of nitrous-oxide production and transport from oceanic low-oxygen zones: A modeling study, *Global Biogeochem. Cy.*, 14, 1353–1370, <https://doi.org/10.1029/1999GB900100>, 2000.
- Suntharalingam, P., Buitenhuis, E., Le Quere, C., Dentener, F., Nevison, C., Butler, J. H., Bange, H. W., and Forster, G.: Quantifying the impact of anthropogenic nitrogen deposition on oceanic nitrous oxide, *Geophys. Res. Lett.*, 39, L07605, <https://doi.org/10.1029/2011GL050778>, 2012.
- Sweeney, C., Gloor, E., Jacobson, A. R., Key, R. M., McKinley, G., Sarmiento, J. L., and Wanninkhof, R.: Constraining global air-sea gas exchange for CO₂ with recent bomb C-14 measurements, *Global Biogeochem. Cy.*, 21, GB2015, <https://doi.org/10.1029/2006GB002784>, 2007.
- Thomalla, S. J., Waldron, H. N., Lucas, M. I., Read, J. F., Anson, I. J., and Pakhomov, E.: Phytoplankton distribution and nitrogen dynamics in the southwest Indian subtropical gyre and Southern Ocean waters, *Ocean Sci.*, 7, 113–127, <https://doi.org/10.5194/os-7-113-2011>, 2011.
- Thompson, R. L., Chevallier, F., Crotwell, A. M., Dutton, G., Langenfelds, R. L., Prinn, R. G., Weiss, R. F., Tohjima, Y., Nakazawa, T., Krummel, P. B., Steele, L. P., Fraser, P., O'Doherty, S., Ishijima, K., and Aoki, S.: Nitrous oxide emissions 1999 to 2009 from a global atmospheric inversion, *Atmos. Chem. Phys.*, 14, 1801–1817, <https://doi.org/10.5194/acp-14-1801-2014>, 2014.
- Vallina, S. M. and Le Quere, C.: Preferential uptake of NH₄⁺ over NO₃⁻ in marine ecosystem models: A simple and more consistent parameterization, *Ecol. Model.*, 218, 393–397, <https://doi.org/10.1016/j.ecolmodel.2008.06.038>, 2008.
- Varela, D. E., Crawford, D. W., Wrohan, I. A., Wyatt, S. N., and Carmack, E. C.: Pelagic primary productivity and upper ocean nutrient dynamics across Subarctic and Arctic Seas, *J. Geophys. Res.-Oceans*, 118, 7132–7152, <https://doi.org/10.1002/2013JC009211>, 2013.
- Varela, M., Bode, A., Fernandez, E., Gonzalez, N., Kitidis, V., Varela, M., and Woodward, E.: Nitrogen uptake and dissolved organic nitrogen release in planktonic communities characterised by phytoplankton size-structure in the Central Atlantic Ocean, *Deep-Sea Res. Pt. I*, 52, 1637–1661, <https://doi.org/10.1016/j.dsr.2005.03.005>, 2005.
- Wafar, M., L'Helguen, S., Raikar, V., Maguer, J., and Corre, P.: Nitrogen uptake by size-fractionated plankton in permanently well-mixed temperate coastal waters, *J. Plankton. Res.*, 26, 1207–1218, <https://doi.org/10.1093/plankt/fbh110>, 2004.
- Wanninkhof, R.: Relationship between wind-speed and gas-exchange over the ocean, *J. Geophys. Res.-Oceans*, 97, 7373–7382, <https://doi.org/10.1029/92JC00188>, 1992.
- Weiss, R. and Price, B.: Nitrous-oxide solubility in water and seawater, *Mar. Chem.*, 8, 347–359, [https://doi.org/10.1016/0304-4203\(80\)90024-9](https://doi.org/10.1016/0304-4203(80)90024-9), 1980.
- Wuchter, C., Abbas, B., Coolen, M. J. L., Herfort, L., van Bleijswijk, J., Timmers, P., Strous, M., Teira, E., Herndl, G. J., Middelburg, J. J., Schouten, S., and Damste, J. S. S.: Archaeal nitrification in the ocean, *P. Natl. Acad. Sci. USA*, 103, 12317–12322, <https://doi.org/10.1073/pnas.0600756103>, 2006.
- Yool, A., Martin, A. P., Fernandez, C., and Clark, D. R.: The significance of nitrification for oceanic new production, *Nature*, 447, 999–1002, <https://doi.org/10.1038/nature05885>, 2007.
- Yoshida, N., Morimoto, H., Hirano, M., Koike, I., Matsua, S., Wada, E., Saino, T., and Hattori, A.: Nitrification rates and N-15 abundances of N₂O and NO₃ in the western North Pacific, *Nature*, 342, 895–897, <https://doi.org/10.1038/342895a0>, 1989.
- Yoshinari, T.: Nitrous oxide in the sea, *Mar. Chem.*, 4, 189–202, 1976.
- Zamora, L. M. and Oschlies, A.: Surface nitrification: A major uncertainty in marine N₂O emissions, *Geophys. Res. Lett.*, 41, 4247–4253, <https://doi.org/10.1002/2014GL060556>, 2014.